


First-principles calculation of anomalous Hall and Nernst conductivity by local Berry phase

Hikaru Sawahata ^{1,2,*}, Naoya Yamaguchi ¹, Susumu Minami ³, and Fumiyuki Ishii ^{1,†}

¹*Nanomaterials Research Institute (NanoMaRi), Kanazawa University, Kanazawa, Ishikawa 920-1192, Japan*

²*PKSHA Technology, Bunkyo-ku, Tokyo 113-0033, Japan*

³*Department of Physics, University of Tokyo, Bunkyo-ku, Tokyo 113-0033, Japan*

 (Received 12 April 2022; revised 8 November 2022; accepted 8 November 2022; published 5 January 2023)

We implemented a finite-difference algorithm for computing anomalous Hall and Nernst conductivity. Based on the expression to evaluate the Berry curvature in an insulating system [J. Phys. Soc. Jpn. **74**, 1674 (2005)], we extended the methods to a metallic system. We calculated anomalous Hall conductivity and Nernst conductivity in a two-dimensional ferromagnetic material FeCl₂ and three-dimensional ferromagnetic transition-metals bcc-Fe, hcp-Co, and fcc-Ni. Our results are comparable to previously reported results computed by the Kubo formula or Wannier representation. To evaluate anomalous Nernst coefficients, the detailed Fermi-energy dependence of the anomalous Hall conductivity is required. The present method will open an efficient thermoelectric material design based on the high-throughput first-principles screening.

DOI: [10.1103/PhysRevB.107.024404](https://doi.org/10.1103/PhysRevB.107.024404)

I. INTRODUCTION

Anomalous Hall effect (AHE) shows Hall conductivity induced by broken time-reversal symmetry based on spontaneous magnetization [1,2]. AHE has an extrinsic mechanism, which originates from impurities [3,4] and an intrinsic mechanism induced by the Berry curvature [5–7]. The Berry curvature is a gauge invariant due to the topology of the electron wave function, and AHE occurs in simple ferromagnetic materials and materials with spin chirality [8,9]. Therefore, the relation between anomalous Hall conductivity and magnetic structure in materials is nontrivial. In an insulating system, AHE has attracted much research attention as a topological effect because it is quantized as a Chern number, which is a topological invariant [10,11].

Anomalous Nernst effect (ANE), which originates from AHE has attracted renewed interest. ANE generates a transverse voltage from a longitudinal temperature gradient due to a transverse electric conductivity through the AHE [2,7,12]. It can be utilized in developing energy-harvesting technology which may provide a simple lateral structure, higher flexibility, and lower production cost [13,14]. Experimental and theoretical studies of ANE have been reported in various magnetic materials [15–41]. Among them, theoretical work predicted large AHE and ANE in the Skyrmion crystal, which has a spin chirality [20,23]. In addition, topological magnets, such as Mn₃Sn [21,22,37], Co₂MnGa [25,27,33], Fe₃X (X = Al, Ga) [30,31], Co₃Sn₂S₂ [26,28,34], and UCoAl [38] are particularly interesting due to their large ANE signal and characteristic low-energy electronics structure including Weyl points.

Anomalous Nernst conductivity (transverse thermoelectric conductivity), which indicates anomalous Nernst thermoelectric conversion efficiency can be evaluated from the chemical potential dependence of anomalous Hall conductivity. The intrinsic component of anomalous Hall conductivity σ_{xy} can be obtained from the Berry curvature $\Omega^n(\mathbf{k})$ as [6,10]

$$\sigma_{xy}(\mu) = \frac{e^2}{h} \sum_n^N \int \frac{d\mathbf{k}^2}{2\pi} \Omega_{nz}(\mathbf{k}) f(\varepsilon_{n\mathbf{k}} - \mu). \quad (1)$$

Here, N , e , h , f , $\varepsilon_{n\mathbf{k}}$, and μ are the electron occupation number, elementary charge, Planck constant, Fermi-Dirac distribution function, band energy with the band index n , wave-vector \mathbf{k} , and Fermi energy, respectively. The Berry curvature $\Omega_n(\mathbf{k})$ is given as

$$\Omega_n(\mathbf{k}) = \nabla \times \mathbf{A}_n, \quad (2)$$

$$\mathbf{A}_n(\mathbf{k}) = -i \langle u_n(\mathbf{k}) | \nabla_{\mathbf{k}} | u_n(\mathbf{k}) \rangle, \quad (3)$$

where \mathbf{A}_n and $u_n(\mathbf{k})$ are the Berry connection and the periodic part of the Bloch states, respectively. In an insulating system, Eq. (1) should be quantized, and it can be described as follows: $\sigma_{xy}(\mu) = (e^2/h)C$ ($C = 0, \pm 1, \pm 2, \dots$). Here, the integer C is the ‘‘Chern number.’’ Anomalous Nernst conductivity α_{xy} can be calculated from the chemical potential dependence of σ_{xy} as follows [42]:

$$\alpha_{xy}(\mu, T) = \frac{1}{e} \int d\varepsilon \sigma_{xy}(\varepsilon) \Big|_{T=0} \frac{\varepsilon - \mu}{T} \left(- \frac{\partial f(\mu)}{\partial \varepsilon} \right). \quad (4)$$

An efficient and simple method to evaluate the chemical potential dependence of σ_{xy} is required for the design of thermoelectric materials based on high-throughput first-principles screening. Previous studies were mainly performed by evaluating the off-diagonal Hall conductivities with Wannier

*sawahata@cphys.s.kanazawa-u.ac.jp

†ishii@cphys.s.kanazawa-u.ac.jp

representation [43–45] or the Kubo formula [46–48]. The former method was implemented in postw90 which is the postprocessing code for the WANNIER90 code [49] and has been widely used in conjunction with many first-principles electronic structure packages. However, some empirical and technical procedures, such as choice of bases and energy window range are required to construct Wannier functions, which are material dependent. In addition, the Wannier representation and the Kubo formula have numerical instability due to the \mathbf{k} -space Dirac monopole [43].

In this paper, we introduce an efficient method for calculating anomalous Hall conductivity σ_{xy} and anomalous Nernst conductivity α_{xy} . We apply the finite-differences expression for Berry curvature [50–52] to metallic systems. One of the method advantages is that σ_{xy} and α_{xy} can be calculated without the construction of Wannier functions demanding the technical or empirical procedure. We implemented our proposed method in the OPENMX code [53], a first-principles calculation package as a post processing code. To confirm the consistency on our proposed method, we calculate σ_{xy} and α_{xy} in two-dimensional ferromagnet FeCl₂ and three-dimensional ferromagnetic transition metals (bcc-Fe, hcp-Co, and fcc-Ni) as a practice. Calculation results successfully reproduced the previous reported ones [32,43,46,47,54,55] obtained from the Kubo formula [46] and Wannier representations [43,44]. Our proposed method will open efficient thermoelectric materials design based on high-throughput first-principles screening. The source code and input files are publicly available on GitHub [56].

II. METHODS

First, we explain a method of computing σ_{xy} in an two-dimensional insulating system, which was proposed by T. Fukui, Y. Hatsugai, and H. Suzuki [50] and T. Fukui and Y. Hatsugai [51].

Let us consider the wave-vector \mathbf{k} at the lattice point on the two-dimensional rectangular Brillouin zone and define its grid interval as δk_x and δk_y along the x and y directions, respectively. The extension to the general lattice system is straightforward. The $N \times N$ overlap matrix on the Brillouin zone is defined as follows:

$$(M_{\mathbf{k},\mathbf{k}+\delta\mathbf{k}})_{mn} = \langle u_m(\mathbf{k}) | u_n(\mathbf{k} + \delta\mathbf{k}) \rangle, \quad (5)$$

and a $U(1)$ link variable is defined as follows:

$$U_{\delta\mathbf{k}}^N(\mathbf{k}) = \det M_{\mathbf{k},\mathbf{k}+\delta\mathbf{k}}. \quad (6)$$

The non-Abelian Berry curvature $\Omega^N(\mathbf{k})$ on the discretized Brillouin zone [50] can be computed using $U_{\delta\mathbf{k}}^N(\mathbf{k})$ as a Berry flux and a local Berry phase [57],

$$\begin{aligned} F^N(\mathbf{k}) &= \text{Im} \ln U_{\delta\mathbf{k}_x}^N(\mathbf{k}) U_{\delta\mathbf{k}_y}^N(\mathbf{k} + \delta\mathbf{k}_x) \\ &\quad \times [U_{\delta\mathbf{k}_x}^N(\mathbf{k} + \delta\mathbf{k}_y)]^{-1} [U_{\delta\mathbf{k}_y}^N(\mathbf{k})]^{-1} \\ &= \text{Im} \ln U_{\delta\mathbf{k}_x}^N(\mathbf{k}) U_{\delta\mathbf{k}_y}^N(\mathbf{k} + \delta\mathbf{k}_x) \\ &\quad \times U_{-\delta\mathbf{k}_x}^N(\mathbf{k} + \delta\mathbf{k}_x + \delta\mathbf{k}_y) U_{-\delta\mathbf{k}_y}^N(\mathbf{k} + \delta\mathbf{k}_y), \quad (7) \end{aligned}$$

where $\delta\mathbf{k}_x = \delta k_x \hat{x}$ and $\delta\mathbf{k}_y = \delta k_y \hat{y}$ [58]. The Berry flux is defined as $F^N(\mathbf{k}) = \Omega_z^N(\mathbf{k}) \delta k_x \delta k_y$. The value of $F^N(\mathbf{k})$ varies in

the range of $-\pi \leq F^N(\mathbf{k}) < \pi$ because $\text{Im} \ln$ is an operation to take the argument of a complex number. This Berry flux takes $\pm\pi$ if a plaquette includes a single Dirac point [7,59]. To compute the Berry flux F , we carried out the contour integration at four wave numbers on the vertices of a plaquette as shown in Fig. 1(a). The anomalous Hall conductivity, σ_{xy} in the insulating system is computed by obtaining the Berry flux on the Brillouin zone $F^N(\mathbf{k})$,

$$\sigma_{xy}(\mu) = \frac{e^2}{h} \frac{1}{2\pi} \sum_{\mathbf{k}} F^N(\mathbf{k}) = \frac{e^2}{h} C. \quad (8)$$

For computing Eq. (7), the matrix size of U must be equal to that in another vertex, i.e., the all occupied number N on vertices of a plaquette must be equal. Therefore, this method can apply only in the insulating system which all occupation numbers N on the vertices of a plaquette are equal.

Next, we expanded the Fukui-Hatsugai-Suzuki method to metallic system. As shown in Fig. 1(b), we consider the case in which any band intersects the Fermi energy.

(i) In the case of occupation numbers N 's on four vertices of a plaquette are equal, we can compute the Berry flux similarly to the case of an insulating system. As shown in Fig. 1(c), we can compute U on each plaquette and obtain Berry flux F .

(ii) In the case that even one occupation number N is different from one of the plaquette, we approximate the Berry flux F by computing the average. Figure 1(d) illustrates the approximation concept for determining the average F . For example, in the case where the occupation numbers on four vertexes are N_1 , N_2 , N_3 , and N_4 , we can obtain the four Berry fluxes $F^{N_1}(\mathbf{k})$, $F^{N_2}(\mathbf{k})$, $F^{N_3}(\mathbf{k})$, and $F^{N_4}(\mathbf{k})$ which are calculated assuming that the all occupation numbers on the four vertices are N_1 , N_2 , N_3 , and N_4 . The approximated Berry flux \bar{F} on this plaquette is approximated by the following equation:

$$\bar{F}(\mathbf{k}) \simeq \frac{1}{4} [F^{N_1}(\mathbf{k}) + F^{N_2}(\mathbf{k}) + F^{N_3}(\mathbf{k}) + F^{N_4}(\mathbf{k})]. \quad (9)$$

Through this approximation, we can compute $\bar{F}(\mathbf{k})$ on all plaquettes, and we can obtain σ_{xy} as

$$\sigma_{xy}(\mu) = \frac{e^2}{h} \sum_{\mathbf{k}} \bar{F}(\mathbf{k}). \quad (10)$$

Confirming the convergence of the above approximation, we compared it with another approximation using the minimum occupation number in Appendix A.

In the case of a three-dimensional simple cubic system, σ_{xy} 's are defined on each k_z . Thus, σ_{xy} in a bulk system is computed by the average along the k_z direction as follows:

$$\sigma_{xy}(\mu) = \frac{1}{N_{k_z}} \sum_{k_z} \sigma_{xy}(\mu, k_z). \quad (11)$$

Here, N_{k_z} is the mesh number along the k_z direction. Through this, σ_{xy} in a three-dimensional system can be computed by applying our method on each k_z .

To evaluate α_{xy} , one need to calculate the μ dependence of σ_{xy} . If one set the maximum occupation number $N = N_{\text{max}}$ corresponding to a chemical potential discussed, one can compute the chemical potential dependence of σ_{xy} by computing

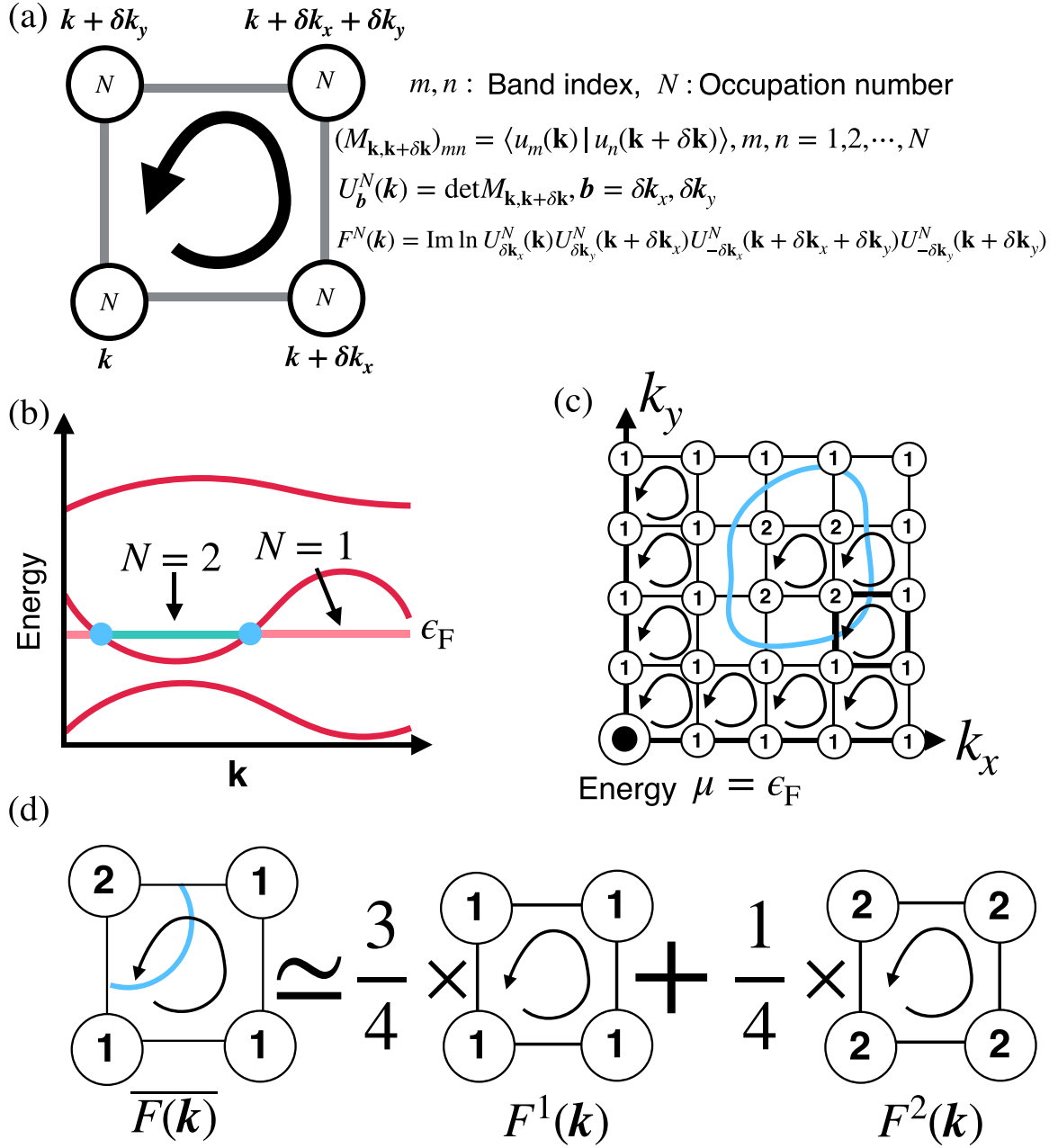


FIG. 1. (a) Computing σ_{xy} in an insulating system. (b) Fermi energy intersecting energy bands. (c) Carrying out contour integration on each plaquette. Except for the plaquette intersecting the Fermi surface, Berry curvature can be computed the same as an insulating system because the occupation numbers N on four vertices are equal to one another. (d) The schematic of an approximation in computing the Berry curvature on the plaquette intersecting the Fermi surface. Assuming occupation numbers on four vertices are equal, one can take the average of the computed Berry curvature.

the overlap matrices once for N_{\max} in Eq. (5). If μ is changed, it is only necessary to recalculate the determinant with $N \leq N_{\max}$ in Eq. (6) from the overlap matrices with $N = N_{\max}$ prepared in advance. Because the computational cost of (6) is much smaller than that of Eq. (5), it is possible to calculate α_{xy} efficiently. This efficiency is shown in Appendix B.

III. COMPUTATIONAL CONDITION

We conducted first-principles calculations based on the noncollinear density functional theory (DFT) based using the

OPENMX code [53]. DFT calculations were performed through the exchange-correlation functional within the generalized gradient approximation [60] and norm-conserving pseudopotentials [61]. The wave functions were expanded by a linear combination of multiple pseudoatomic orbitals [62,63]. The spin-orbit interaction was included by using total-angular-momentum-dependent pseudopotentials [64]. For FeCl_2 , the cutoff energy for a charge density of 500 Ry, a \mathbf{k} -point sampling of $20 \times 20 \times 1$, and lattice constant of 3.475 Å were used. A set of pseudoatomic orbital basis functions was specified as $\text{Fe}6.0\text{S-}s2p3d3f1$ and $\text{Cl}7.0\text{-}s3p3d2$, where 6.0 and 7.0

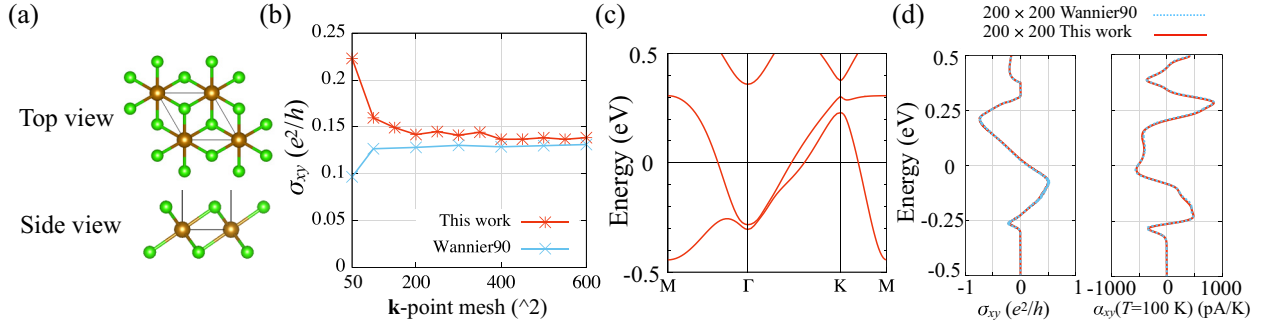


FIG. 2. (a) Crystal structure of FeCl_2 . (b) \mathbf{k} -mesh dependence of the σ_{xy} at the Fermi energy. (c) Band structure of FeCl_2 . (d) Chemical potential dependence of the σ_{xy} and α_{xy} . Blue and red solid line points correspond to the present calculation results and results obtained from WANNIER90, respectively. The high-symmetry points are $\Gamma(0, 0, 0)$, $M(1/2, 0, 0)$, and $K(1/3, 1/3, 0)$.

are the cutoff radii (in bohrs) of each element, respectively. S stands for a soft pseudopotential, and the integers after s , p , d , and f indicates the radial multiplicity of each angular momentum component. These computational conditions are the same as those reported previously study [32]. For bcc-Fe, the cutoff energy for a charge density of 300 Ry, a \mathbf{k} -point sampling of $36 \times 36 \times 36$, and lattice constant of 2.87 \AA were used. A set of pseudoatomic orbital basis functions was specified as $\text{Fe}6.0S\text{-}s3p3d3f1$. For details of hcp-Co and fcc-Ni, see Appendix C.

IV. RESULTS AND DISCUSSION

A. Two-dimensional ferromagnetic FeCl_2

Here, our method is applied for the two-dimensional ferromagnetic FeCl_2 , which has a simple electronic structure and a large ANE [32]. Figure 2(a) shows the schematic crystal structure of FeCl_2 , where six Cl atoms connect each Fe atom. This material is known as a ferromagnetic two-dimensional material with half-metallicity [32,65,66].

Figure 2(b) shows the \mathbf{k} -mesh dependence of σ_{xy} at the Fermi energy. We found that σ_{xy} converged to $0.14 (e^2/h)$ with a 200×200 \mathbf{k} -mesh, and its value converged within about 10% with a 100×100 \mathbf{k} -mesh. This convergence with a small number of \mathbf{k} -mesh is similar to the previous first-principles calculation [67]. Compared to the results of WANNIER90, our proposed method exhibit a very small difference less than $0.014 (e^2/h)$ where the \mathbf{k} -mesh is greater than 200×200 at the Fermi energy. One of the factors for this convergence is that the ratio of the plaquette number with the approximation of Eq. (9), decreased from 12% to 3% whereas the \mathbf{k} -mesh increased from 50×50 to 200×200 .

Next, we confirm the chemical potential dependence of the σ_{xy} and α_{xy} . Figure 2(c) shows the electronic band structure for FeCl_2 . A simple band structure without degenerate points near the Fermi energy is noticeable in this case. Figure 2(d) shows the chemical potential dependence of the σ_{xy} at 0 K and α_{xy} at 100 K. The \mathbf{k} -mesh of $200 \times 200 \times 1$ were used for both calculations. Our calculation results [blue solid line in Fig. 2(d)] reproduce completely those obtained from the Wannier representations. Table I shows the mean absolute error of σ_{xy} with respect to μ , and we confirmed convergence with increasing \mathbf{k} -mesh. Therefore, we conclude

that our method can reproduce the results obtained from the Wannier representations in a simple electronic structure case.

B. Three-dimensional ferromagnetic materials

Next, let us perform our method in a three-dimensional ferromagnetic system. We calculated the σ_{xy} and α_{xy} for bcc-Fe, hcp-Co, and fcc-Ni as a typical example. Here, we focused on bcc-Fe (Fig. 3(a) [68]) (for hcp-Co and fcc-Ni, see Appendix C). In Table II, we compared the σ_{xy} for bcc-Fe at the Fermi energy for the present paper with a previous study. We can see that our calculation results converge to approximately $\sigma_{xy} \simeq 750 \text{ S/cm}$ as similarly reported in the previous theoretical calculation.

Figure 3(b) shows the \mathbf{k} -mesh dependence of the σ_{xy} at the Fermi energy. The σ_{xy} converged with, at least, the \mathbf{k} -mesh of $200 \times 200 \times 200$, and its value converged within about 10% with $100 \times 100 \times 100$ \mathbf{k} -mesh. Compared to the results of WANNIER90, our proposed method exhibits a very small difference less than 6 S/cm, where the \mathbf{k} -mesh is finer than $400 \times 400 \times 400$ at the Fermi energy. One of the factors for this convergence is that the ratio of the plaquette number with the approximation of Eq. (9), decreased from 22% to 3% whereas the \mathbf{k} -mesh increased from $100 \times 100 \times 100$ to $700 \times 700 \times 700$. We can conclude that our method could reproduce the σ_{xy} at a specific chemical potential.

Finally, we discuss the chemical potential dependence of the σ_{xy} and α_{xy} for bcc-Fe. Table III shows the mean absolute error of σ_{xy} with respect to μ . Compared to the two-dimensional system, the convergence of the chemical

TABLE I. Mean absolute error of σ_{xy} with respect to μ in FeCl_2 . The errors were estimated as the difference from converged \mathbf{k} -mesh 200×200 . The energy range is -0.5 to 0.5 eV. ‘‘Min.’’ means minimum occupation number. For details, see Appendix A in the main text.

\mathbf{k} -mesh	Error (e^2/h) Eq. (9)	Error (e^2/h) Min.
50×50	0.043	0.067
100×100	0.012	0.047

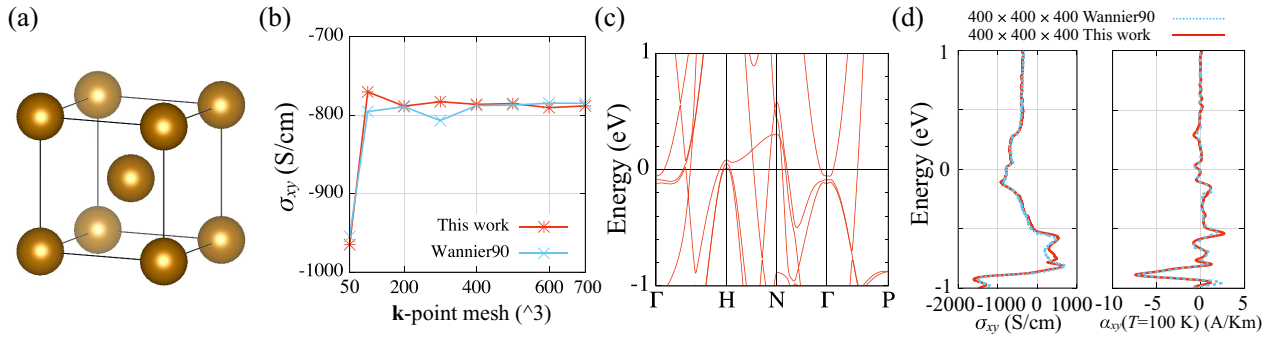


FIG. 3. (a) Crystal structure of bcc-Fe. (b) \mathbf{k} -mesh dependence of the σ_{xy} at the Fermi energy. (c) Band structure of bcc-Fe. (d) Chemical potential dependence of the σ_{xy} and α_{xy} . Blue and red solid line points correspond to the present calculation results and results obtained from WANNIER90, respectively. The high-symmetry points are $\Gamma(0, 0, 0)$, $H(1/2, -1/2, 1/2)$, $N(0, 0, 1/2)$, and $P(1/4, 1/4, 1/4)$.

potential dependence of σ_{xy} with increasing \mathbf{k} -mesh is slower than two-dimensional results. Figures 3(c) and 3(d) show the band structure of bcc-Fe and the chemical potential dependence of the σ_{xy} at 0 K and α_{xy} at 100 K, respectively. Compared to the two-dimensional system, the correspondence of σ_{xy} between our method and the Wannier representation is slightly lowered at the specific energy region from -1.0 to -0.5 eV. This numerical error may originate from an entangled or degenerate electronic structure because the bcc-Fe system has many degenerate points stemming from point nodes [69]. However, due to the smearing of the Fermi-Dirac distribution function, this inconsistency decreases as the temperature increases. In fact, as shown in Fig. 3, it shows that our α_{xy} of bcc-Fe at 100 K results are almost consistent with those calculated by WANNIER90. We safely conclude that our method has enough accuracy for evaluating α_{xy} in a finite temperature. At low temperature, it is difficult to obtain α_{xy} , and we can improve it by using smeared σ_{xy} (see Appendix D).

V. CONCLUSION

In this paper, we expanded the Fukui-Hatsugai-Suzuki method to a metallic system to improve the efficiency in calculation of σ_{xy} and α_{xy} in magnetic materials. Calculating an average of the Berry flux on the all \mathbf{k} -mesh plaquette

TABLE II. Comparison of this paper and previous ones for the σ_{xy} in bcc-Fe.

Refs.	σ_{xy} (S/cm)
Yao <i>et al.</i> [46]	751
Wang <i>et al.</i> [43]	756.76
Lee <i>et al.</i> [47]	750
Exp. [70]	1032
This paper (100×100×100)	770
This paper (200×200×200)	788
This paper (300×300×300)	782
This paper (400×400×400)	786
This paper (500×500×500)	785
This paper (600×600×600)	790
This paper (700×700×700)	788

with respect to each vertex, makes it possible to estimate σ_{xy} in partially occupied cases. We also demonstrated the calculations of σ_{xy} and α_{xy} by using this method in a typical two-dimensional ferromagnetic material FeCl_2 and three-dimensional magnetic transition-metal bcc-Fe, hcp-Co, and fcc-Ni. The σ_{xy} in FeCl_2 with a simple band structure completely reproduced the calculation results obtained from the Wannier representation and exhibited fast conversion with a rough \mathbf{k} -mesh. Whereas, in three-dimensional transition-metal cases, the consistency is slightly dropped in a specific energy range because of a complicated band structure; however, we find a good agreement for anomalous Nernst conductivity at a finite temperature. The present paper will give us a more efficient calculation method for the AHE and ANE without some technical and empirical procedures, such as those constructing Wannier functions. High-throughput first-principles screening based on this method will be a useful tool for thermoelectric materials design.

ACKNOWLEDGMENTS

We thank K. Shibata for discussions. This work was partly supported by JSPS KAKENHI Grants No. JP20J13011, No. JP20K15115, No. JP20K22479, No. JP22K04862, and No. JP22K14587. This work was partly supported by Japan Science and Technology Agency (JST) as part of SICORP, Grant No. JPMJSC21E3. The computation was mainly carried out using the computer facilities at ISSP, The University of Tokyo, and RIIT, Kyushu University. The computations in this research were partially performed using the Fujitsu PRIMERGY CX400M1/CX2550M5 (Oakbridge-CX) in the

TABLE III. Mean absolute error of σ_{xy} with respect to μ in bcc-Fe. Energy range is -1.5 eV to 1.5 eV. The errors were estimated as the difference from converged \mathbf{k} -mesh $400 \times 400 \times 400$. Min. means minimum occupation number. For details, see Appendix A in the main text.

\mathbf{k} -mesh	Error (S/cm) Eq. (9)	Error (S/cm) Min.
100×100×100	114	148
200×200×200	43	51

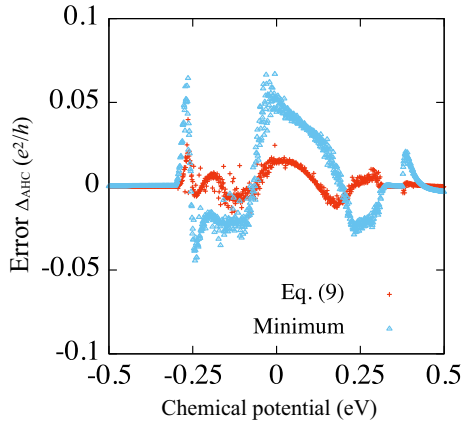


FIG. 4. The chemical potential dependence of calculated error for σ_{xy} in FeCl_2 : $\Delta_{\text{AHC}} = \sigma_{xy}^{\text{Eq. (10)}} - \sigma_{xy}^{\text{postw90}}$, where $\sigma_{xy}^{\text{Eq. (10)}}$ and $\sigma_{xy}^{\text{postw90}}$ were values obtained from our implementation based on Eq. (10) and postw90, respectively. The red plus symbol shows the results by using Eq. (9) for \bar{F} . The blue triangle shows the results by using $F^{\min(N_1-N_4)}$ for \bar{F} . For details, see Appendix A in the main text. The \mathbf{k} -mesh of 200×200 was used.

Information Technology Center, The University of Tokyo. Crystal structures were drawn by VESTA [68].

APPENDIX A: APPROXIMATION ON BERRY FLUX ON THE FERMI SURFACE

To check the validity of the method computing Berry flux F with Eq. (9), we calculated F as the case of minimum occupation number in the plaquettes, i.e., $F = F^{\min(N_1-N_4)}$. Figure 4 shows the error of σ_{xy} compared to the result of WANNIER90 for two-dimensional FeCl_2 . The result using Eq. (9) is more convergent than the result using the minimum occupation number. For example, at the chemical potential $\mu = 0$ eV,

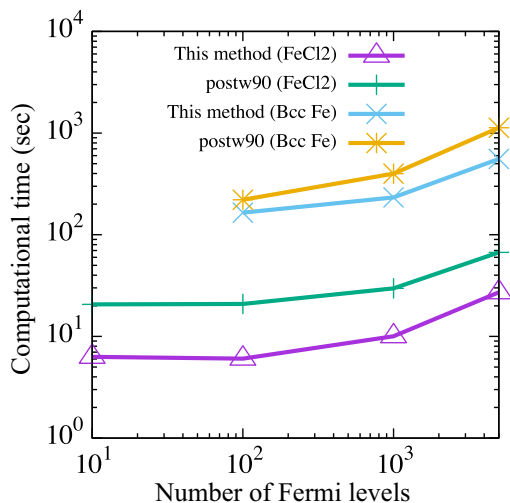


FIG. 5. Computational time of our method and postw90 in the WANNIER90 package for the FeCl_2 system with 100×100 \mathbf{k} -point mesh and the bcc-Fe system with $100 \times 100 \times 100$ \mathbf{k} -point mesh. Note that the computational time of postw90 does not include that consumed by “wannierization.”

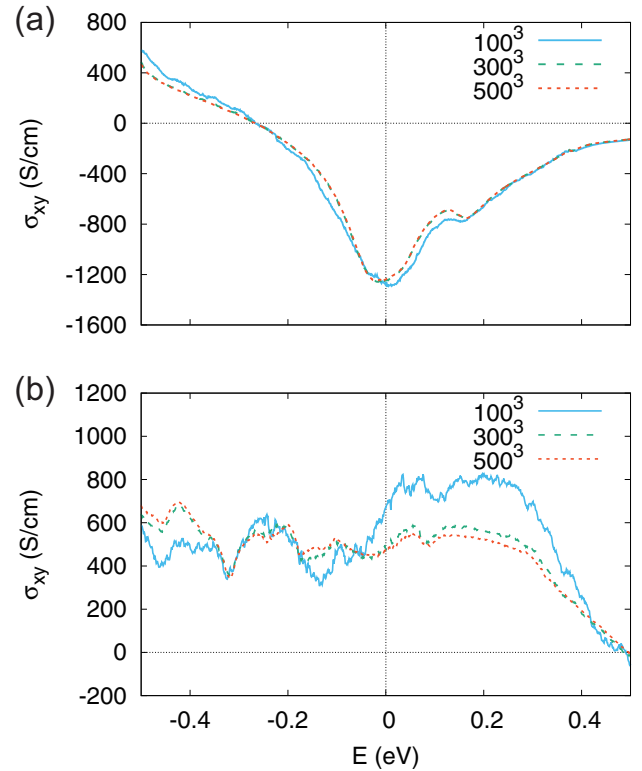


FIG. 6. Chemical potential dependence of σ_{xy} for (a) hcp-Co, and (b) fcc-Ni. Blue-solid, green-dashed, and red-dot lines correspond to the \mathbf{k} -mesh of $100 \times 100 \times 100$, $300 \times 300 \times 300$, and $500 \times 500 \times 500$, respectively.

the minimum occupation case has the error $\Delta_{\text{AHC}} = 0.044$ (e^2/h) whereas the result of Eq. (9) has the error $\Delta_{\text{AHC}} = 0.014$ (e^2/h).

APPENDIX B: COMPUTATIONAL TIME OF MULTIPLE FERMI LEVELS

We compared computational times of our proposed method with postw90 in the WANNIER90 package for the FeCl_2 system to validate the efficiency of our method. We performed calculations of FeCl_2 and bcc-Fe cases with eight nodes of a supercomputer with AMD EPYC 7702 [2.0 GHz (64 core) $\times 2$] and measured the computational times with the flat MPI including the 1024 and 256 MPI processes, respectively. To get the chemical potential dependence of σ_{xy} , calculations of scanning the chemical potential (i.e., Fermi level) are demanded. In this comparison of computational times, we considered the scanning calculations as practical cases. As shown in Fig. 5, for both FeCl_2 and bcc-Fe, the required computational times were shorter than postw90 for all the cases with respect to the number of scans of the Fermi level. Therefore, we can conclude that our method is more efficient than postw90.

APPENDIX C: ANOMALOUS HALL CONDUCTIVITY FOR hcp-Co AND fcc-Ni

We also calculated the σ_{xy} for ferromagnetic hcp-Co and fcc-Ni. For fcc-Ni, the cutoff energy for a charge density

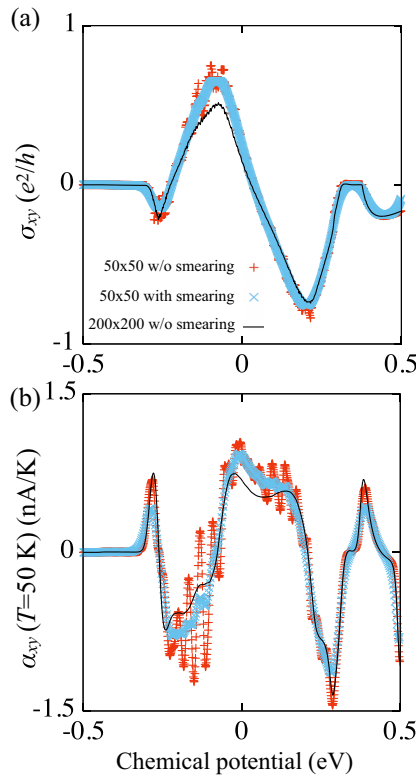


FIG. 7. Chemical potential dependence of (a) σ_{xy} and (b) α_{xy} at $T = 50$ K in FeCl_2 . Red plus symbol indicates results with 50×50 meshes without smearing. The blue x symbol indicates $\tilde{\sigma}_{xy}^{T_s=100\text{K}}(\mu)$ and α_{xy} at $T = 50$ K calculated from $\tilde{\sigma}_{xy}^{T_s=100\text{K}}(\mu)$. The black lines indicate results with 200×200 without smearing. $\tilde{\sigma}_{xy}^{T_s}$ even with a poor mesh improves α_{xy} .

of 300 Ry, a \mathbf{k} -point sampling of $32 \times 32 \times 32$, and lattice constant of $a = 3.56$ Å were used. A set of pseudoatomic orbital basis functions was specified as $\text{Ni}6.0-s3p2d2f1$. For hcp-Co, the cutoff energy for a charge density of 300 Ry, a

\mathbf{k} -point sampling of $24 \times 24 \times 18$, lattice constant of $a = 2.50$, and $c = 4.07$ Å were used. A set of pseudoatomic orbital basis functions was specified as $\text{Co}6.0-s3p2d2f1$. Figure 6 shows the chemical potential dependence of σ_{xy} for hcp-Co and fcc-Ni. We found that the results converged for a \mathbf{k} -point mesh of $300 \times 300 \times 300$. Our calculation results well reproduce the previous studies [54,55].

APPENDIX D: SMEARING EFFECT AT LOW TEMPERATURE

Generally, a quite computational cost is required to obtain the convergence value of σ_{xy} and α_{xy} at low temperatures. Smearing for σ_{xy} and α_{xy} could be a promising method to reduce that computational cost. Figure 7(a) shows the chemical potential dependence of σ_{xy} for FeCl_2 . The red dot and black solid line represent σ_{xy} calculated with the \mathbf{k} -point mesh of 50×50 and 200×200 , respectively. The blue dot represents smeared σ_{xy} with calculated with a \mathbf{k} -point mesh of 50×50 . We performed smearing σ_{xy} at smearing temperature T_s by using the Fermi-Dirac function $f(\epsilon, T_s)$ as

$$\tilde{\sigma}_{xy}^{T_s}(\mu) = \int d\epsilon \left(-\frac{\partial f(\epsilon, \mu, T_s)}{\partial \epsilon} \right) \sigma_{xy}(\epsilon), \quad (\text{D1})$$

and the integration is performed by the trapezoidal rule. We can see that spiky peaks are reduced in $\tilde{\sigma}_{xy}^{T_s}(\mu)$. We obtained α_{xy} using $\tilde{\sigma}_{xy}$ as

$$\alpha_{xy}(\mu, T) = \frac{1}{e} \int d\epsilon \tilde{\sigma}_{xy}^{T_s}(\epsilon) \frac{\epsilon - \mu}{T} \left(-\frac{\partial f(\mu)}{\partial \epsilon} \right). \quad (\text{D2})$$

We also calculated α_{xy} as shown in Fig. 7(b). α_{xy} calculated with a \mathbf{k} -point mesh of 50×50 shows oscillation along with chemical potential due to the numerical convergence of σ_{xy} . In contrast, the oscillation is suppressed by using $\tilde{\sigma}_{xy}^{T_s}(\mu)$. Using $\tilde{\sigma}_{xy}^{T_s}$, we can improve the convergence of α_{xy} .

-
- [1] E. H. Hall, *Proc. Phys. Soc. London* **4**, 325 (1880).
[2] N. Nagaosa, J. Sinova, S. Onoda, A. H. MacDonald, and N. P. Ong, *Rev. Mod. Phys.* **82**, 1539 (2010).
[3] J. Smit, *Physica* **24**, 39 (1958).
[4] L. Berger, *Phys. Rev. B* **2**, 4559 (1970).
[5] M. V. Berry, *Proc. R. Soc. London, Ser. A* **392**, 45 (1984).
[6] M. Kohmoto, *Ann. Phys.* **160**, 343 (1985).
[7] D. Xiao, M.-C. Chang, and Q. Niu, *Rev. Mod. Phys.* **82**, 1959 (2010).
[8] K. Ohgushi, S. Murakami, and N. Nagaosa, *Phys. Rev. B* **62**, R6065 (2000).
[9] S. Nakatsuji, N. Kiyohara, and T. Higo, *Nature (London)* **527**, 212 (2015).
[10] D. J. Thouless, M. Kohmoto, M. P. Nightingale, and M. den Nijs, *Phys. Rev. Lett.* **49**, 405 (1982).
[11] C.-Z. Chang, J. Zhang, X. Feng, J. Shen, Z. Zhang, M. Guo, K. Li, Y. Ou, P. Wei, L.-L. Wang, Z.-Q. Ji, Y. Feng, S. Ji, X. Chen, J. Jia, X. Dai, Z. Fang, S.-C. Zhang, K. He *et al.*, *Science* **340**, 167 (2013).
[12] D. Xiao, Y. Yao, Z. Fang, and Q. Niu, *Phys. Rev. Lett.* **97**, 026603 (2006).
[13] Y. Sakuraba, *Scr. Mater.* **111**, 29 (2016).
[14] M. Mizuguchi and S. Nakatsuji, *Sci. Tech. Adv. Mater.* **20**, 262 (2019).
[15] W.-L. Lee, S. Watauchi, V. L. Miller, R. J. Cava, and N. P. Ong, *Phys. Rev. Lett.* **93**, 226601 (2004).
[16] T. Miyasato, N. Abe, T. Fujii, A. Asamitsu, S. Onoda, Y. Onose, N. Nagaosa, and Y. Tokura, *Phys. Rev. Lett.* **99**, 086602 (2007).
[17] Y. Pu, D. Chiba, F. Matsukura, H. Ohno, and J. Shi, *Phys. Rev. Lett.* **101**, 117208 (2008).
[18] Y. Sakuraba, K. Hasegawa, M. Mizuguchi, T. Kubota, S. Mizukami, T. Miyazaki, and K. Takanashi, *Appl. Phys. Express* **6**, 033003 (2013).
[19] K. Hasegawa, M. Mizuguchi, Y. Sakuraba, T. Kamada, T. Kojima, T. Kubota, S. Mizukami, T. Miyazaki, and K. Takanashi, *Appl. Phys. Lett.* **106**, 252405 (2015).
[20] Y. P. Mizuta and F. Ishii, *Sci. Rep.* **6**, 28076 (2016).

- [21] M. Ikhlas, T. Tomita, T. Koretsune, M.-T. Suzuki, D. Nishio-Hamane, R. Arita, Y. Otani, and S. Nakatsuji, *Nat. Phys.* **13**, 1085 (2017).
- [22] G.-Y. Guo and T.-C. Wang, *Phys. Rev. B* **96**, 224415 (2017).
- [23] Y. P. Mizuta, H. Sawahata, and F. Ishii, *Phys. Rev. B* **98**, 205125 (2018).
- [24] S. Minami, F. Ishii, Y. P. Mizuta, and M. Saito, *Appl. Phys. Lett.* **113**, 032403 (2018).
- [25] A. Sakai, Y. Mizuta, A. Nugroho, R. Sihombing, T. Koretsune, M. Suzuki, N. Takemori, R. Ishii, D. Nishio-Hamane, R. Arita, P. Goswami, and S. Nakatsuji, *Nat. Phys.* **14**, 1119 (2018).
- [26] E. Liu, Y. Sun, N. Kumar, L. Muechler, A. Sun, L. Jiao, S.-Y. Yang, D. Liu, A. Liang, Q. Xu, J. Kroder, V. Süß, H. Borrmann, C. Shekhar, Z. Wang, C. Xi, W. Wang, W. Schnelle, S. Wirth, Y. Chen *et al.*, *Nat. Phys.* **14**, 1125 (2018).
- [27] S. N. Guin, K. Manna, J. Noky, S. J. Watzman, C. Fu, N. Kumar, W. Schnelle, C. Shekhar, Y. Sun, J. Gooth, and C. Felser, *NPG Asia Mater.* **11**, 16 (2019).
- [28] S. N. Guin, P. Vir, Y. Zhang, N. Kumar, S. J. Watzman, C. Fu, E. Liu, K. Manna, W. Schnelle, J. Gooth, C. Shekhar, Y. Sun, and C. Felser, *Adv. Mater.* **31**, 1806622 (2019).
- [29] J. Xu, W. A. Phelan, and C.-L. Chien, *Nano Lett.* **19**, 8250 (2019).
- [30] A. Sakai, S. Minami, T. Koretsune, T. Chen, T. Higo, Y. Wang, T. Nomoto, M. Hirayama, S. Miwa, D. Nishio-Hamane, F. Ishii, R. Arita, and S. Nakatsuji, *Nature (London)* **581**, 53 (2020).
- [31] S. Minami, F. Ishii, M. Hirayama, T. Nomoto, T. Koretsune, and R. Arita, *Phys. Rev. B* **102**, 205128 (2020).
- [32] R. Syariati, S. Minami, H. Sawahata, and F. Ishii, *APL Mater.* **8**, 041105 (2020).
- [33] K. Sumida, Y. Sakuraba, K. Masuda, T. Kono, M. Kakoki, K. Goto, W. Zhou, K. Miyamoto, Y. Miura, T. Okuda, and A. Kimura, *Commun. Mater.* **1**, 89 (2020).
- [34] H. Yang, W. You, J. Wang, J. Huang, C. Xi, X. Xu, C. Cao, M. Tian, Z.-A. Xu, J. Dai, and Y. Li, *Phys. Rev. Mater.* **4**, 024202 (2020).
- [35] Z. Shi, S.-J. Xu, L. Ma, S.-M. Zhou, and G.-Y. Guo, *Phys. Rev. Appl.* **13**, 054044 (2020).
- [36] M. Hirschberger, L. Spitz, T. Nomoto, T. Kurumaji, S. Gao, J. Masell, T. Nakajima, A. Kikkawa, Y. Yamasaki, H. Sagayama, H. Nakao, Y. Taguchi, R. Arita, T.-H. Arima, and Y. Tokura, *Phys. Rev. Lett.* **125**, 076602 (2020).
- [37] T. Chen, T. Tomita, S. Minami, M. Fu, T. Koretsune, M. Kitatani, I. Muhammad, D. Nishio-Hamane, R. Ishii, F. Ishii, R. Arita, and S. Nakatsuji, *Nat. Commun.* **12**, 572 (2021).
- [38] T. Asaba, V. Ivanov, S. M. Thomas, S. Y. Savrasov, J. D. Thompson, E. D. Bauer, and F. Ronning, *Sci. Adv.* **7**, eabf1467 (2021).
- [39] B. He, C. Şeahin, S. R. Boona, B. C. Sales, Y. Pan, C. Felser, M. E. Flatté, and J. P. Heremans, *Joule* **5**, 3057 (2021).
- [40] H. Nakamura, S. Minami, T. Tomita, A. A. Nugroho, and S. Nakatsuji, *Phys. Rev. B* **104**, L161114 (2021).
- [41] T. Chen, S. Minami, A. Sakai, Y. Wang, Z. Feng, T. Nomoto, M. Hirayama, R. Ishii, T. Koretsune, R. Arita, and S. Nakatsuji, *Sci. Adv.* **8**, eabk1480 (2022).
- [42] Y. P. Mizuta and F. Ishii, *JPS Conf. Proc.* **3**, 017035 (2014).
- [43] X. Wang, J. R. Yates, I. Souza, and D. Vanderbilt, *Phys. Rev. B* **74**, 195118 (2006).
- [44] M. G. Lopez, D. Vanderbilt, T. Thonhauser, and I. Souza, *Phys. Rev. B* **85**, 014435 (2012).
- [45] S. S. Tsirkin, *npj Comput. Mater.* **7**, 33 (2021).
- [46] Y. Yao, L. Kleinman, A. H. MacDonald, J. Sinova, T. Jungwirth, D.-S. Wang, E. Wang, and Q. Niu, *Phys. Rev. Lett.* **92**, 037204 (2004).
- [47] C.-C. Lee, Y.-T. Lee, M. Fukuda, and T. Ozaki, *Phys. Rev. B* **98**, 115115 (2018).
- [48] G. Jin, D. Zheng, and L. He, *J. Phys.: Condens. Matter* **33**, 325503 (2021).
- [49] G. Pizzi, V. Vitale, R. Arita, S. Blgel, F. Freimuth, G. Géranton, M. Gibertini, D. Gresch, C. Johnson, T. Koretsune, J. Ibañez-Azpiroz, H. Lee, J.-M. Lihm, D. Marchand, A. Marrazzo, Y. Mokrousov, J. I. Mustafa, Y. Nohara, Y. Nomura, L. Paulatto *et al.*, *J. Phys.: Condens. Matter* **32**, 165902 (2020).
- [50] T. Fukui, Y. Hatsugai, and H. Suzuki, *J. Phys. Soc. Jpn.* **74**, 1674 (2005).
- [51] T. Fukui and Y. Hatsugai, *J. Phys. Soc. Jpn.* **76**, 053702 (2007).
- [52] W. Feng, J. Wen, J. Zhou, D. Xiao, and Y. Yao, *Comput. Phys. Commun.* **183**, 1849 (2012).
- [53] T. Ozaki *et al.*, OpenMX: Open source package for Material eXplorer, <http://www.openmx-square.org/>.
- [54] H.-R. Fuh and G.-Y. Guo, *Phys. Rev. B* **84**, 144427 (2011).
- [55] J. Weischenberg, F. Freimuth, S. Blügel, and Y. Mokrousov, *Phys. Rev. B* **87**, 060406 (2013).
- [56] <https://github.com/hikaruri/OMXsigmaxy>.
- [57] R. D. King-Smith and D. Vanderbilt, *Phys. Rev. B* **47**, 1651 (1993).
- [58] This transformation uses $\text{Im} \ln M^{-1} = \text{Im} \ln M^\dagger$.
- [59] H. Sawahata, N. Yamaguchi, H. Kotaka, and F. Ishii, *Jpn. J. Appl. Phys.* **57**, 030309 (2018).
- [60] J. P. Perdew, K. Burke, and M. Ernzerhof, *Phys. Rev. Lett.* **77**, 3865 (1996).
- [61] D. R. Hamann, M. Schlüter, and C. Chiang, *Phys. Rev. Lett.* **43**, 1494 (1979).
- [62] T. Ozaki, *Phys. Rev. B* **67**, 155108 (2003).
- [63] T. Ozaki and H. Kino, *Phys. Rev. B* **69**, 195113 (2004).
- [64] G. Theurich and N. A. Hill, *Phys. Rev. B* **64**, 073106 (2001).
- [65] V. V. Kulish and W. Huang, *J. Mater. Chem. C* **5**, 8734 (2017).
- [66] H. Zheng, J. Zheng, C. Wang, H. Han, and Y. Yan, *J. Magn. Magn. Mater.* **444**, 184 (2017).
- [67] J. Kübler and C. Felser, *Phys. Rev. B* **85**, 012405 (2012).
- [68] K. Momma and F. Izumi, *J. Appl. Crystallogr.* **44**, 1272 (2011).
- [69] D. Gosálbez-Martínez, I. Souza, and D. Vanderbilt, *Phys. Rev. B* **92**, 085138 (2015).
- [70] P. N. Dheer, *Phys. Rev.* **156**, 637 (1967).